Biogeosciences

Open Access

Influence of meteorology and anthropogenic pollution on chemical flux divergence of the NO–NO$_2$–O$_3$ triad above and within a natural grassland canopy

D. Plake[1,*], M. Sörgel[1], P. Stella[1,**], A. Held[2], and I. Trebs[1,***]

[1]Max Planck Institute for Chemistry, Biogeochemistry Department, P.O. Box 3060, 55020 Mainz, Germany
[2]University of Bayreuth, Atmospheric Chemistry, Bayreuth, Germany
[*]now at: Air Monitoring Department, UCL Umwelt Control Labor GmbH, 44536 Lünen, Germany
[**]now at: AgroParisTech, UMR INRA/AgroParisTech SAD-APT, Paris, France
[***]now at: Luxembourg Institute of Science and Technology, Environmental Research and Innovation (ERIN) Department, 4422 Belvaux, Luxembourg

Correspondence to: I. Trebs (ivonne.trebs@list.lu)

Abstract. The detailed understanding of surface–atmosphere exchange fluxes of reactive trace gases is a crucial precondition for reliable modelling of processes in atmospheric chemistry. Plant canopies significantly impact the atmospheric budget of trace gases. In the past, many studies focused on taller forest canopies or crops, where the bulk plant material is concentrated in the uppermost canopy layer. However, within grasslands, a land-cover class that globally covers vast terrestrial areas, the canopy structure is fundamentally different, as the main biomass is concentrated in the lowest part of the canopy. This has obvious implications for aerodynamic in-canopy transport, and consequently also impacts on global budgets of key species in atmospheric chemistry such as nitric oxide (NO), nitrogen dioxide (NO$_2$) and ozone (O$_3$).

This study presents for the first time a comprehensive data set of directly measured in-canopy transport times and aerodynamic resistances, chemical timescales, Damköhler numbers, trace gas and micrometeorological measurements for a natural grassland canopy (canopy height = 0.6 m). Special attention is paid to the impact of contrasting meteorological and air chemical conditions on in-canopy transport and chemical flux divergence. Our results show that the grassland canopy is decoupled throughout the day. In the lowermost canopy layer, the measured transport times are fastest during nighttime, which is due to convection during nighttime and a stable stratification during daytime in this layer. The inverse

was found in the layers above. During periods of low wind speed and high NO$_x$ (NO+NO$_2$) levels, the effect of canopy decoupling on trace gas transport was found to be especially distinct. The aerodynamic resistance in the lowermost canopy layer (0.04–0.2 m) was around 1000 s m^{-1}, which is as high as values determined previously for the lowest metre of an Amazonian rain forest canopy. The aerodynamic resistance representing the bulk canopy was found to be more than 3–4 times higher than in forests. Calculated Damköhler numbers (ratio of transport and chemical timescales) suggest a strong flux divergence for the NO–NO$_2$–O$_3$ triad within the canopy during daytime. During that time, the timescale of NO$_2$ uptake by plants ranged from 90 to 160 s and was the fastest relevant timescale, i.e. faster than the reaction of NO and O$_3$. Thus, our results reveal that grassland canopies of similar structure exhibit a strong potential to retain soil-emitted NO due to oxidation and subsequent uptake of NO$_2$ by plants. Furthermore, photo-chemical O$_3$ production was observed above the canopy, which was attributed to a deviation from the NO–NO$_2$–O$_3$ photostationary state by a surplus of NO$_2$ due to oxidation of NO, by e.g. peroxy radicals. The O$_3$ production was one order of magnitude higher during high NO$_x$ than during low NO$_x$ periods and resulted in an underestimation of the O$_3$ deposition flux measured with the EC method.

1 Introduction

Nitric oxide (NO) and nitrogen dioxide (NO_2) play a crucial role in air chemistry as they act as key catalysts for ozone (O_3) production and are therefore involved in the generation of hydroxyl radicals (OH) (Crutzen, 1973). The most significant tropospheric source of O_3 is initiated by photochemical dissociation of NO_2 and subsequent reaction of the oxygen (O) atom with molecular oxygen:

$$NO_2 + hv\,(\lambda < 420\,nm) \rightarrow NO + O(^3P) \qquad (R1)$$

$$O(^3P) + O_2 + M \rightarrow O_3 + M. \qquad (R2)$$

In the case that O_3 is present, it may oxidize NO and re-form NO_2:

$$O_3 + NO \xrightarrow{k_3} NO_2 + O_2 \qquad (R3)$$

In the absence of additional reactions, R1–R3 represent a null cycle. Besides R1–R3, NO is oxidized by peroxy radicals (HO_2+RO_2), which constitutes an important net O_3 production pathway in the troposphere (Warneck, 2000).

Dry deposition to terrestrial surfaces, especially to plant canopies, is an important sink for tropospheric O_3 and NO_2. The uncertainties of dry deposition estimates are substantially higher for NO_2, because its net ecosystem exchange can be bi-directional depending on the ambient NO_2 levels (Lerdau et al., 2000). O_3 instead is exclusively deposited to surfaces. In contrast, NO is known to be mainly net emitted from nearly all soil types. Biogenic NO soil emissions contribute about 20 % to the global NO_x ($NO+NO_2$) emissions (IPCC, 2013), highlighting the need of detailed investigations on NO_x soil–atmosphere exchange.

A major challenge for studies investigating surface–atmosphere exchange fluxes of these reactive trace gases is the presence of plant canopies. These significantly modify the aerodynamic properties of the surface and, thus, alter trace gas exchange fluxes. Most previous studies focused on taller canopies such as forests. However, grassland canopies represent a highly important land cover class covering globally 41 % and Europe-wide 19 % of the terrestrial land surface (Suttie et al., 2005; Kasanko et al., 2011). In contrast to forests, grasslands feature the main bulk plant area density near the soil (e.g. Ripley and Redman, 1976; Jäggi et al., 2006), accompanied with mean distances between plant elements of only some millimetres (Aylor et al., 1993). Organized coherent structures govern turbulence dynamics within and above plant canopies (Finnigan, 2000). The mean in-canopy transport is slower than above the canopy (e.g. Nemitz et al., 2009). This modification of in-canopy transport has important implications for global atmospheric chemistry. Plant canopies and the soil below are biologically actively emitting and taking up reactive trace gases, and conditions

within canopies may provide sufficient time for fast chemical reactions (Nemitz et al., 2009). Subsequently, they modify surface exchange fluxes (e.g. Rinne et al., 2012). For instance, ammonia can be released by a part of the canopy and taken up by another (Nemitz et al., 2000; Denmead et al., 2007). In addition, recapturing of NO_2 originating from biogenic soil NO emissions after reaction with O_3 within plant canopies (Rummel et al., 2002) is accounted for in global models by a so-called canopy reduction factor for NO_x (Yienger and Levy, 1995). However, these estimates are based on only one single experiment in an Amazonian rain forest (Bakwin et al., 1990), and a subsequent model analysis (Jacob and Wofsy, 1990). Canopy reduction for grasslands and other ecosystems has not been experimentally studied up to now. The contrasting canopy structure of grassland and forest ecosystems highlights the need for a detailed analysis and an evaluation of the suggested NO_x canopy reduction factor of e.g. 64 % by Yienger and Levy (1995) for temperate grassland.

Net ecosystem exchange fluxes are typically measured at a certain height above the canopy. They rely on the constant flux layer assumption (e.g. Swinbank, 1968), which however, may be violated for reactive trace gases within or just above the vegetation. To assess the potential chemical divergence of exchange fluxes, the Damköhler number (DA) has commonly been applied (e.g. Rinne et al., 2012). DA is calculated as the ratio of the transport time (τ_{tr}) and the characteristic chemical timescale (τ_{ch}):

$$DA = \frac{\tau_{tr}}{\tau_{ch}}. \qquad (1)$$

Hence, DA above unity indicates that chemical reactions occur significantly faster than the transport (flux divergence), whereas DA smaller than 0.1 indicates the reverse case. The range in between is commonly addressed as a critical range, where an impact of chemistry cannot be excluded (Stella et al., 2013).

In this paper, we present directly measured transport times, chemical timescales and corresponding Damköhler numbers for three layers above and within a natural grassland canopy under contrasting meteorological and air chemical conditions. For the first time, such a comprehensive analysis involving trace gas and micrometeorological measurements is made for a grassland canopy. Furthermore, the consequences of in-canopy processes for NO_x canopy reduction and simultaneously measured O_3 deposition fluxes will be discussed.

2 Material and methods

2.1 Site description

We performed an intensive field experiment from July to September 2011 at the estate of the Mainz Finthen Airport in Rhineland-Palatinate, Germany (further details given in

Plake and Trebs, 2013; Plake et al., 2014; Moravek et al., 2014, 2015). The vegetation at the site was nutrient-poor grassland with a mean canopy height (h_c) of 0.6 m and a leaf area index (LAI) of $4.8\,\mathrm{m^2\,m^{-2}}$. A list of species and an LAI profile are given in Plake et al. (2014), with the latter indicating a high biomass density below 0.2 m corresponding to 85 % of the total LAI. Topographically located on a plateau 150 m above the Rhine valley, the site is located about 9 km south-west of the city centre of Mainz. The site is surrounded by villages and motorways in a distance of 2 to 6 km and 4 to 15 km, respectively. The surrounding area is mainly characterized by agricultural use for vineyards, orchards and crops. The fetch is largest in southwestern direction without significant anthropogenic pollution sources.

2.2 Experimental setup

A vertical Thoron (Tn) profile system was operated at $z_1 = 0.04$, $z_2 = 0.2$ and $z_3 = 0.8$ m for the direct determination of transport times (for details see Plake and Trebs, 2013). Vertical profiles of NO, NO_2, O_3 and CO_2 were measured at z_1, z_2, z_3 and additionally at $z_4 = 4.0$ m by a system described in detail by Plake et al. (2014). Briefly, NO was measured by detection of the chemiluminescence produced during the reaction of NO and O_3 (TEI 42iTL Thermo Scientific, Waltham, USA). NO_2 was photolytically converted to NO by exposure of the sample air to a blue light converter (BLC, Droplet Measurement Technologies, Boulder, USA). O_3 mixing ratios were measured with a UV-absorption analyser (TEI-49i, Thermo Scientific, Waltham, USA). The efficiency of the photolytic conversion of NO_2 to NO was determined by a back-titration procedure involving the reaction of O_3 with NO using a gas phase titration system (SYCOS K-GPT, Ansyco GmbH, Karlsruhe, Germany). Details on the sampling schedule and time resolution of the trace gas profiles system are described in Plake et al. (2014).

This study is based on simultaneous operation of both vertical profile systems at identical heights and, thus, focuses on the period from 19 August to 26 September 2011 when both systems were operational. Vertical profiles of temperature (HMT337, Vaisala, Helsinki, Finland), wind speed and direction (WS425, Vaisala, Helsinki, Finland) were installed at 0.2, 0.8, 1.5, 2.5, 4.0 m. Soil temperature (107L, Campbell Scientific Inc., Logan, USA) was measured at -0.02 m. Global radiation (G) and the NO_2 photolysis frequency (j_{NO_2}) were measured at a height of 2.5 m with a net radiometer (CNR1, Kipp & Zonen, Delft, Netherlands), and a filter radiometer (Meteorology Consult GmbH, Königstein, Germany), respectively. The data of temperature, wind and radiation were recorded by a data logger (CR3000, Campbell Scientific) every 10 s. A 3-D sonic anemometer (CSAT-3, Campbell Scientific) placed at $z_{ref} = 3.0$ m measured 3-D wind and temperature at 20 Hz and the data were recorded by a CR3000 data logger. The friction velocity (u_*) and stability functions (z/L) were computed using the TK3 software

(see Mauder and Foken, 2011). Eddy covariance fluxes of O_3 were simultaneously measured and are described in detail by Plake et al. (2014).

2.3 Theory

The data analysis was carried out for three individual layers (L_{1-3}), which are named in ascending order starting at the soil surface. Hence, L_1 is the lowermost canopy layer between the corresponding measurement heights z_{1-2} ($\Delta z(L_1) = 0.16$ m), L_2 the upper canopy layer between z_{2-3} ($\Delta z(L_2) = 0.6$ m), and L_3 the layer above the canopy between z_3 and z_{ref} ($\Delta z(L_3) = 2.2$ m). As shown in Plake et al. (2014) the vertical trace gas gradients between z_{ref} and z_4 were negligible, allowing the use of mixing ratios measured at z_4 for L_3.

2.3.1 Chemical timescales

The overall chemical timescale τ_{ch} (in s) of the NO–NO_2–O_3 triad (Lenschow, 1982) was calculated for each layer (L_i, $i = 1, 2, 3$) as

$$\tau_{ch}(L_i) = 2 \Big/ \Big\{ j_{NO_2}(L_i)^2 + k_3(L_i)^2 \times \big(N_{O_3}(L_i) \tag{2}$$
$$- N_{NO}(L_i))^2 + 2 j_{NO_2}(L_i) \times k_3(L_i) \times \big(N_{O_3}(L_i)$$
$$+ N_{NO}(L_i) + 2N_{NO_2}(L_i)\big) \Big\}^{0.5},$$

where N_{O_3}, N_{NO} and N_{NO_2} are the number densities (in molecules $\mathrm{cm^{-3}}$) of O_3, NO and NO_2 for L_{1-3}, and k_3 the reaction rate constant of Reaction (R3) (in $\mathrm{cm^3\,molecule^{-1}\,s^{-1}}$) according to Atkinson et al. (2004). Geometric means of the number densities at z_{1-4} were used in Eq. (2) to account for non-linear profiles – e.g. $N_{NO}(L_1) = \sqrt{N_{NO}(z_1) \times N_{NO}(z_2)}$.

Equation (2) gives the chemical timescale of Reactions (R1) and (R3) derived from the O_3 chemical-budget equation, i.e. considering only the reactions between O_3, NO and NO_2 and not taking into account reactions of other compounds (e.g. peroxy radicals and VOCs). It is defined as the time at which the mixing ratio of one of the compounds significantly changes from its initial value when reacting with the other ones. It can also be seen as the time required for reaching a new photostationary state following a change in O_3, NO or NO_2 mixing ratios, or the reaction rate constants j_{NO_2} and k_3 (see Ganzeveld et al., 2012). The underlying assumptions are:

– only source and sink terms of the "triad" are considered, which means other reactions (e.g. $RO_2 + NO$) are not included;

– covariance terms and other budget terms i.e. horizontal and vertical advection, flux divergence and change in O_3 mixing ratio $d[O_3]/dt$ are neglected.

2.3.2 NO$_2$ photolysis within the canopy

The data gaps in the measured time series of j_{NO_2} (in s^{-1}) above the canopy were filled using the parameterization of j_{NO_2} as a function of G (in W m^{-2}) by Trebs et al. (2009). This approach was also used to parameterize in-canopy j_{NO_2} from a vertical in-canopy profile of G. The latter was calculated as a function of the LAI profile using the method of Monsi and Saeki (1953):

$$G\,(\text{LAI}) = G_0 \times \exp^{(-k_{ex} \times \text{LAI})}, \tag{3}$$

where G_0 (in W m^{-2}) is the above-canopy G and k_{ex} is the dimensionless extinction coefficient of the canopy. In this study, the extinction coefficient of barley ($k_{ex} = 0.69$ by Monteith and Unsworth, 1990) was used. First $G\,(\text{LAI})$ was deduced and then converted into j_{NO_2}. Finally, geometric means of j_{NO_2} were calculated for $j_{NO_2}(L_{1-3})$.

2.3.3 Transport times

For L_3, height-integrated transport times $\tau_{tr}(L_3)$ (in s) were derived by multiplying the aerodynamic resistance $R_a(L_3)$ (e.g. Hicks et al., 1987; Erisman et al., 1994) with the layer thickness $\Delta z(L_3)$ (see Stella et al., 2013):

$$\tau_{tr}\,(L_3) = R_a(L_3) \times \Delta z(L_3) \tag{4}$$

$$R_a(L_3) = \frac{1}{\kappa \times u_*}\left[\ln\left(\frac{z_{ref}-d}{z_3-d}\right) - \Psi_H\left(\frac{z_{ref}-d}{L}\right) + \Psi_H\left(\frac{z_3-d}{L}\right)\right], \tag{5}$$

where κ is the von Kàrmàn constant ($= 0.4$), d the displacement height ($d = 0.75 \times h_c$), Ψ_H the stability correction function for heat (Foken, 2008) and L the Obukhov length.

In the canopy, $\tau_{tr}(L_i, i = 1, 2)$ were derived from the vertical Tn profiles (Lehmann et al., 1999; Plake and Trebs, 2013):

$$\tau_{tr}\,(L_i) = \ln\left[\frac{C_{Tn_{z_l}}(L_i)}{C_{Tn_{z_u}}(L_i)}\right] / \lambda \tag{6}$$

where $C_{Tn_{z_l}}$ and $C_{Tn_{z_u}}$ are the measured Tn concentrations (in Bq m^{-3}) at the lower (z_l) and upper (z_u) heights of L_i, and λ the radioactive decay rate $\lambda = \ln 2 / T_{0.5} = 0.0125$ s^{-1} (Hänsel and Neumann, 1995).

3 Results

3.1 Meteorological conditions and mixing ratios

During the field experiment, low and high NO$_x$ periods occurred that were directly coupled to the wind direction and could be attributed to two contrasting synoptic conditions characterized by different wind speeds (see Moravek et al.,
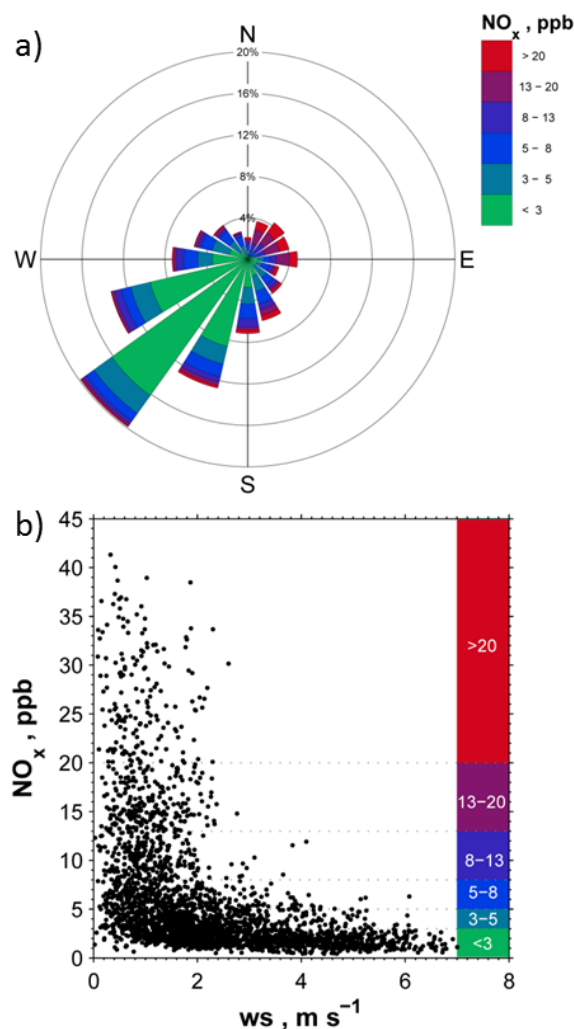
Figure 1. (a) Frequency distribution of wind direction related to NO$_x$ mixing ratios; **(b)** NO$_x$ mixing ratios as function of wind speed at the Mainz Finthen grassland site.

2015). Figure 1a displays the dominance of southwesterly winds at the site during 45 % of the field experiment and their relation to relatively low NO$_x$ levels (< 3 ppb). Contrastingly, winds from the northeastern sector were characterized by high NO$_x$ levels often above 13 ppb (Fig. 1a). High NO$_x$ episodes (up to 40 ppb) were accompanied with low wind speed (< 3 m s^{-1}) and low NO$_x$ (< 5 ppb) with wind speeds above 3 m s^{-1} as shown in Fig. 1b. O$_3$ levels exhibited the opposite dependency on wind speed, while the measured CO$_2$ levels generally showed a similar pattern for high and low NO$_x$ levels.

For further data analysis, defined criteria made it possible to account for these specific relationships. In order to clearly separate entire days (24 h) of contrasting conditions from each other, the criteria were defined as low NO$_x$ or high NO$_x$ periods when (i) the mean daytime wind speed was > 3 m s^{-1} and the wind direction mainly ranged between 180 and 270°,
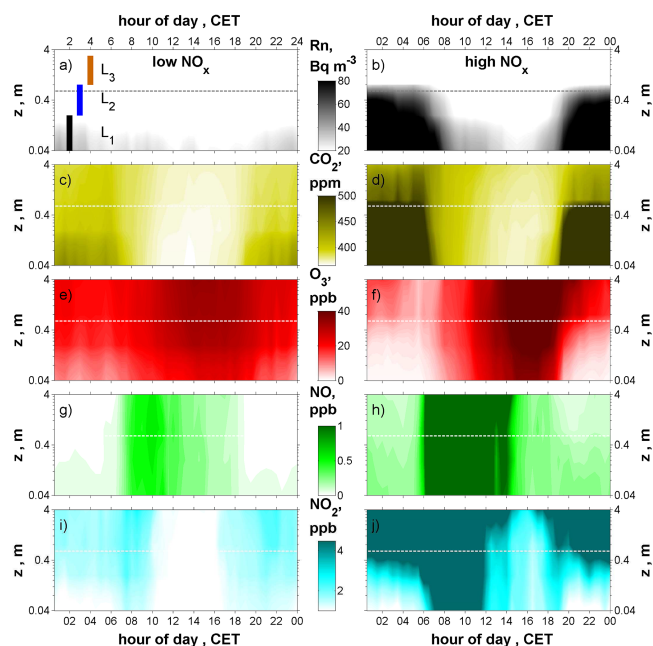
Figure 2. Time height cross-sections indicating the median vertical distribution of **(a, b)** Rn, **(c, d)** CO_2, **(e, f)** O_3, **(g, h)** NO and **(i, j)** NO_2 during low NO_x (left panels) and high NO_x (right panels) conditions at the Mainz Finthen grassland site. The canopy height (dotted line) and L_{1-3} are also shown. The plots were made using the *contourf* function of MATLAB.

or (ii) the mean daytime wind speed was $< 3\,\mathrm{m\,s^{-1}}$ and the wind direction was mainly outside 180–270°, respectively. The wind direction definition was fulfilled during 96 % of the low NO_x periods and during 84 % of the high NO_x periods. Following these criteria, we identified 11 and 9 days as low and high NO_x periods, respectively, which were analysed separately.

3.2 Vertical profiles of trace gases

Since the wind field drives vertical exchange of scalars such as trace gases between vegetation and the atmosphere (Finnigan, 2000), it affects their vertical distribution. Passive tracers such as Rn and CO_2 are used especially at nighttime as indicators for vertical exchange processes within plant canopies (e.g. Trumbore et al., 1990; Nemitz et al., 2009). Generally, nighttime wind speeds during the low and high NO_x periods were accordingly higher and lower, respectively. This was reflected by the in-canopy concentrations of both Rn and CO_2 (Fig. 2a–d). During nighttime when both gases are exclusively emitted by soil, a rather weak enrichment within the canopy (Fig. 2a, c) reflected higher wind speeds and, thus, enhanced exchange during the low NO_x periods. In comparison, during the high NO_x periods a strong in-canopy CO_2 and Rn accumulation was observed (Fig. 2b, d). During daytime, photosynthesis prohibits the use of CO_2 as passive tracer, whereas Rn profiles are still useful as no

biological processes such as stomatal uptake affect its concentration (Lehmann et al., 1999). The vertical exchange is generally enhanced during daytime causing dilution of the in-canopy Rn concentrations, which was especially pronounced during the low NO_x periods (Fig. 2a) and was less evident during the high NO_x periods (Fig. 2b) with generally lower wind speeds.

The vertical distribution of O_3 (Fig. 2e, f) reflected a typical pattern with lower mixing ratios closer to the ground and higher mixing ratios above. The diurnal O_3 maximum occurred during the afternoon around 16:00 CET (= UTC +1). Nevertheless, in the low NO_x periods the diurnal O_3 maximum was much less pronounced compared to the high NO_x periods with 35 and 50 ppb, respectively. Furthermore, characteristic vertical O_3 distributions were observed during the low and high NO_x periods. Nighttime O_3 gradients were less pronounced during the low NO_x than during the high NO_x periods. Median in-canopy values of O_3 were 10–20 ppb and were 20–25 ppb above the canopy during the low NO_x periods (Fig. 2e). During the high NO_x periods 1–6 ppb of O_3 were measured in the canopy and 10–25 ppb above the canopy (Fig. 2f).

During both the low and the high NO_x periods, significantly enhanced NO mixing ratios prevailed during the morning hours from 06:00 to 14:00 CET (Fig. 2g, h) with median diurnal maxima of 0.6 and 7.2 ppb, respectively, both occurring at 10:00 CET (not visible in Fig. 2h due to scaling). The NO mixing ratios decreased afterwards to approach nighttime minima. These were characterized by small vertical NO gradients during both periods. During low NO_x nights, NO appeared to be mainly present in the in-canopy air layer, with median mixing ratios at z_1 and z_2 of ≤ 0.1 ppb. The median values at z_1 and z_2 during the high NO_x periods were ≤ 0.3 ppb, respectively.

NO_2 mixing ratios were generally found to increase with height (Fig. 2i, j), featuring significantly stronger vertical differences during the high NO_x periods. Similar to NO, also NO_2 mixing ratios were enhanced throughout the profile during the morning hours of both, low and high NO_x periods, with corresponding values of 1–2.5 ppb and 6–14 ppb, respectively. At nighttime, comparable NO_2 mixing ratios of around 1 ppb prevailed during both periods at z_1. NO_2 showed stronger gradients above the canopy during the high NO_x periods. The diurnal NO_2 minima during low and high NO_x periods were observed between 12–16 CET and 14–16 CET, respectively.

3.3 Vertical profiles of chemical timescales

The obtained values for τ_{ch} were generally higher during nighttime than during daytime (Fig. 3a, d, g) and increased from L_3 to L_1. The validity of our applied criteria for separation between low and high NO_x periods is shown by the median values (brown and green lines) that nearly adjoin the interquartile range of the overall data set. Significantly higher
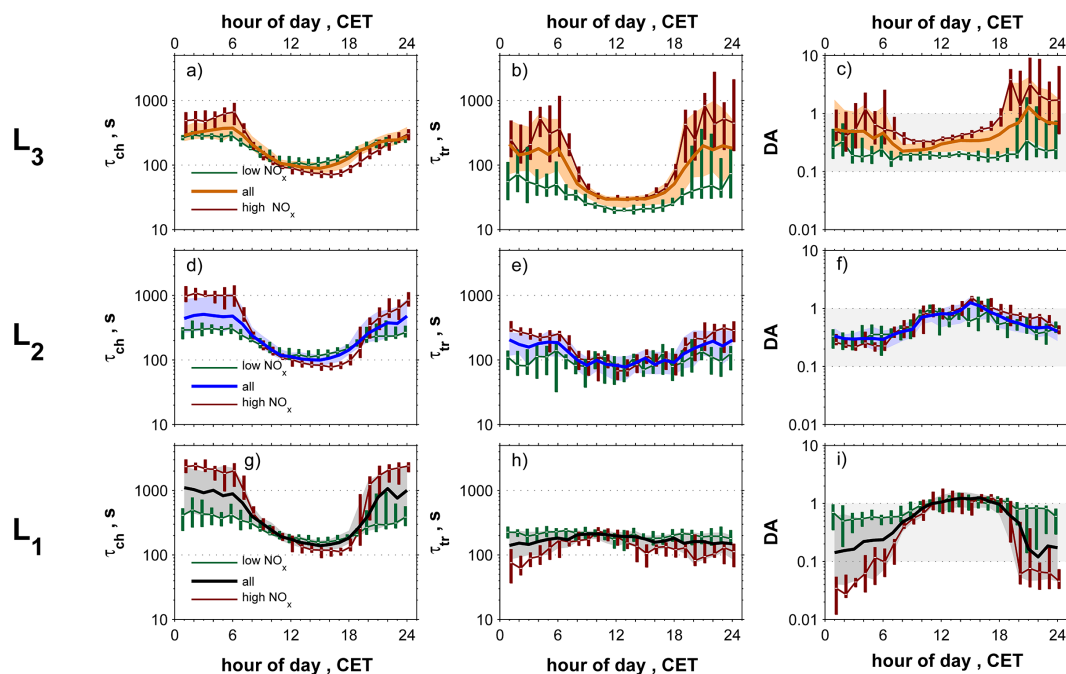
Figure 3. Diurnal courses of **(a, d, g)** $\tau_{ch}(L_{1-3})$, **(b, e, h)** $\tau_{tr}(L_{1-3})$ and **(c, f, i)** $DA(L_{1-3})$ considering all data from 19 August to 26 September 2011 (medians and shaded interquartile ranges) and the low NO_x and high NO_x periods (green and brown medians and interquartile boxes) at the Mainz Finthen grassland site.

τ_{ch} values prevailed during nighttime of the high NO_x periods, ranging from 300 to 2500 s in L_{1-3}. In contrast, low NO_x periods were characterized by τ_{ch} of 250–800 s in L_{1-3}. However, during daytime τ_{ch} was within 100–200 s in L_{1-3} for both periods. During the low NO_x periods τ_{ch} values were slightly higher compared to the high NO_x periods.

3.4   Vertical profiles of transport times

The median $\tau_{tr}(L_3)$ of all data (Fig. 3b) was one order of magnitude smaller during noon than at midnight with 30 and 200 s, respectively. As for τ_{ch} (Sect. 3.3), also in the case of τ_{tr} the medians of the low and high NO_x periods adjoined the interquartile range of the overall data set. For example, $\tau_{tr}(L_3)$ in the low NO_x periods never exceeded $\tau_{tr}(L_3)$ in the high NO_x periods (see Fig. 3b). The difference of $\tau_{tr}(L_3)$ between noon and midnight was largest in the high NO_x and smallest during the low NO_x periods with 470 and 40 s, respectively. Compared to L_{1-2} (Fig. 3e, h), the extreme values of the entire τ_{tr} data set were found above the canopy in L_3. The overall τ_{tr} minimum occurred during daytime of the low NO_x periods, and the maximum during nighttime of the high NO_x periods in L_3.

The diurnal course of $\tau_{tr}(L_2)$ from the entire data set in Fig. 3e exhibited a similar pattern as $\tau_{tr}(L_3)$, with higher $\tau_{tr}(L_2)$ during nighttime than during daytime. Representative nighttime and daytime values were 200 and 100 s, respec-

tively, and a similar nighttime separation between the low and high NO_x periods as in Fig. 3b is observed.

In contrast, both diurnal $\tau_{tr}(L_1)$ medians representing all data and the high NO_x periods (Fig. 3h) were slightly higher during daytime between 08:00 and 13:00 CET than at nighttime with around 200 and 75–175 s, respectively. During the low NO_x periods, the median $\tau_{tr}(L_1)$ was relatively constant throughout the day with about 200 s. The pattern of $\tau_{tr}(L_1)$ was generally opposite to L_{2-3}, with faster $\tau_{tr}(L_1)$ in the high NO_x periods than in the low NO_x periods.

3.5   Vertical profiles of Damköhler numbers

The values for $DA(L_3)$ presented in Fig. 3c were generally smaller during daytime than during nighttime. They exhibited a diurnal minimum of 0.2 and a maximum of 1.3 at 08:00 and 21:00 CET, respectively. During the low NO_x periods, the difference of the $DA(L_3)$ median ($0.2 < DA(L_3) < 0.3$) to a DA of unity was highest, whereas in the high NO_x periods $DA(L_3)$ remained at higher median values ($0.3 < DA(L_3) < 3.9$).

In contrast, the diurnal course of $DA(L_2)$ in Fig. 3f exhibited its maximum of 1.25 at 15:00 CET and featured nighttime minima of about 0.3. The difference in $DA(L_2)$ between the low and high NO_x periods was not as pronounced as for $DA(L_3)$. This was most obvious from 15:00 to 24:00 CET with lower $DA(L_2)$ in the low NO_x periods. Hence, both
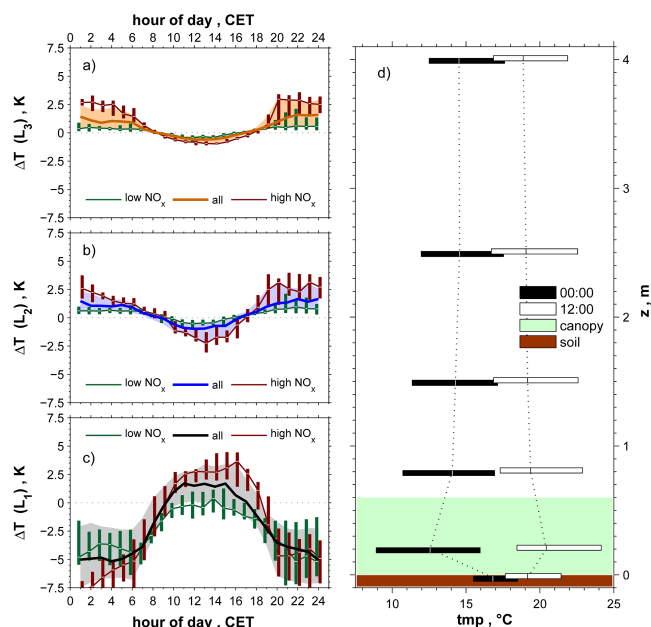
Figure 4. (a–c) Diurnal courses of measured $\Delta T(L_{1-3})$ considering all data from 19 August to 26 September 2011 (medians and shaded interquartile ranges) and the low and high NO_x periods (green and brown medians and interquartile ranges); note: $\Delta T(L_1, L_3)$ do not fully cover L_1 and L_3 (Sect. 2.3) due to availability of measurements (Sect. 2.2); **(a)** $\Delta T(L_3)$: 2.5–0.8 m; **(b)** $\Delta T(L_2)$: 0.8–0.2 m; **(c)** $\Delta T(L_1)$: 0.2 to -0.02 m (soil temperature). **(d)** Median vertical temperature profiles and interquartile boxes representing the thermal stratification at 00:00 and 12:00 CET considering all data from 19 August to 26 September 2011 at the Mainz Finthen grassland site.

$DA(L_{2,3})$ values throughout the day were within or above the critical range for DA under all conditions.

Interestingly, the diurnal course of $DA(L_1)$ (Fig. 3i) nearly mirrored that of $DA(L_3)$, with highest and lowest DA during daytime and nighttime, respectively. The diurnal median of $DA(L_1)$ partly exhibited values below 0.1 (transport dominates) during nighttime of the high NO_x periods, values above unity (chemistry dominates) from 12:00 to 17:00 CET under all conditions, and between 0.1 and unity during nighttime in the overall data set and in the low NO_x periods.

4 Discussion

4.1 Transport times and resistances

4.1.1 Thermal stratification

The diurnal courses of the temperature differences $\Delta T(L_{1-3})$ in Fig. 4a–c describe the stability in each layer. They clearly indicate contrasting stability conditions in L_1 and L_{2-3}. During daytime, negative values of $\Delta T(L_{2-3})$ reflected unstable conditions, while positive

$\Delta T(L_1)$ reflected stable conditions. In contrast, at nighttime these conditions were reversed. Similar diurnal cycles of stratifications are observed for other canopies (see Jacobs et al., 1994; Kruijt et al., 2000; Nemitz et al., 2000), and are known to decouple the lower canopy from the air layers above (see Fig. 4d). Canopy coupling regimes are typically classified according to the detection of coherent structures in high frequency time series of scalars such as temperature (e.g. Foken et al., 2012; Dupont and Patton, 2012). In our data set $\Delta T(L_1)$ was used to explain why $\tau_{tr}(L_1)$ was generally smaller, i.e. transport was faster during nighttime than during daytime (Fig. 3h). The soil released stored heat as thermal plumes during nighttime that drove an in-canopy nighttime convection, which reached up to the height of the temperature inversion as found by Dupont and Patton (2012) or Jacobs et al. (1994). The $\tau_{tr}(L_1)$ maximum of 200 s from 08:00 to 13:00 CET could accordingly be attributed to positive $\Delta T(L_1)$ values at that time indicating a stable stratification. The thermal stratification was stronger during the high NO_x periods and weaker during the low NO_x periods in all layers (Fig. 4a–c). This was caused by higher wind speeds during the low NO_x periods causing increased turbulence and mixing that yielded smaller vertical temperature differences.

4.1.2 Aerodynamic resistances and transport times

Aerodynamic resistances above (R_a) and within the canopy (R_{ac}) are considered as important input variables for modelling studies on surface–atmosphere exchange fluxes. They can be derived from the transport times through a layer, normalized by the layer thickness ($R_{a(c)} = \tau_{tr}/\Delta z$). In cases when the thicknesses of two layers under consideration differ, the effectiveness of transport can be represented by the corresponding aerodynamic resistances. On the other hand, transport times are required to evaluate the influence of chemical reactions on fluxes (e.g. DA).

Typically, R_{ac} values are parameterized as a function of u_* and LAI (e.g. van Pul and Jacobs, 1994; Personne et al., 2009). These parameterizations are based on experiments above, e.g. crops such as maize (van Pul and Jacobs, 1994), and consider a vertically homogeneous leaf distribution (Personne et al., 2009). However, this approximation may differ substantially within grassland canopies, as their structure is characterized by high biomass density in the lowest layer (see Sect. 2.1).

The importance of our results is underlined by the direct assessment of measured R_{ac} values. From Eq. (6) we can assess R_{ac} for different canopy layers (L_1, L_2 and for the whole canopy ($\tau_{tr}(z_1, z_3)$; $\Delta z = z_3 - z_1$)) of the grassland (see Fig. 5). In the lowermost canopy layer, $R_{ac}(L_1)$ was generally highest with medians of 900 to 1000 s m^{-1} during nighttime and 1000 to 1300 s m^{-1} during daytime (Fig. 5). In comparison, Gut et al. (2002) found the aerodynamic resistance in the lowest metre of an Amazonian rain forest
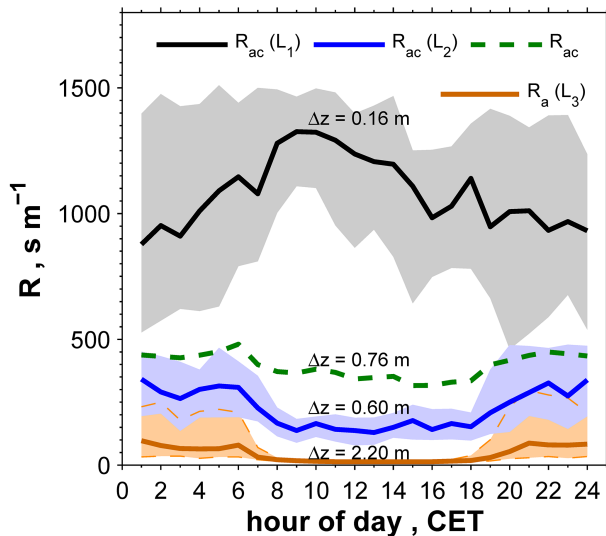
Figure 5. Diurnal courses of in-canopy aerodynamic resistances for each individual canopy layer ($R_{ac}(L_1)$, $R_{ac}(L_2)$) and for the entire grassland canopy ($R_{ac} = \frac{\tau_{tr}(L_1) + \tau_{tr}(L_2)}{z_3 - z_1}$) at the Mainz Finthen site (median and shaded interquartile ranges). For comparison, the aerodynamic resistance above the canopy is also displayed ($R_a(L_3)$). The layer thickness (Δz) is indicated. The plot includes all data from 19 August until 26 September 2011.

canopy in a similar range with $600\,\mathrm{s\,m^{-1}}$ during nighttime and $1700\,\mathrm{s\,m^{-1}}$ during daytime, showing the same diurnal pattern.

As found for the transport times, the diurnal course of R_{ac} in the upper layers mirrored that of the lowermost layer (Fig. 5). In the upper canopy, the median of $R_{ac}(L_2)$ typically ranged around $300\,\mathrm{s\,m^{-1}}$ during nighttime and around $150\,\mathrm{s\,m^{-1}}$ during daytime. In comparison, above the canopy the median of $R_a(L_3)$ (Eq. 5) was substantially lower with around 80 and $15\,\mathrm{s\,m^{-1}}$ during nighttime and daytime, respectively. Consequently, the aerodynamic resistances in and above the canopy ($R_{ac}(L_{1,2})$ and $R_a(L_3)$) differed by almost two orders of magnitude during daytime, and by one order of magnitude during nighttime. Accordingly, the efficiency of aerodynamic transport decreased with decreasing height, even if the transport times were occasionally shorter in L_1 compared to L_3. R_{ac} for the entire canopy (Fig. 5) reflects the sum of the measured transport times divided by the entire layer thickness ($\Delta z = z_3 - z_1$) and can be considered as equivalent to a weighted average of $R_{ac}(L_1)$ and $R_{ac}(L_2)$. R_{ac} ranged in-between $R_{ac}(L_1)$ and $R_{ac}(L_2)$ with $440\,\mathrm{s\,m^{-1}}$ during nighttime and $360\,\mathrm{s\,m^{-1}}$ during daytime. The opposite diurnal courses of both $R_{ac}(L_1)$ and $R_{ac}(L_2)$ have an impact on R_{ac}, which in turn showed a smaller diurnal variation. As L_2 contained around 80 % of the layer thickness between z_1 and z_3 (see Fig. 5), R_{ac} was closer to $R_{ac}(L_2)$.

The median transport time through the 0.6 m high natural grassland canopy (also referred to as "canopy flushing time")

was presented in the related study of Plake and Trebs (2013) for the same experiment. It was measured using the vertical thoron profile between z_1 and z_3 (Eq. 6). The canopy flushing time is consistent with the sum of $\tau_{tr}(L_1)$ and $\tau_{tr}(L_2)$ in this paper (see Fig. 7) and represents the in-canopy layer down to $0.07 \times h_c$ (z_1/h_c). It was determined to be $\leq 6\,\mathrm{min}$ exhibiting only small daytime/nighttime variation. Simon et al. (2005) reported canopy flushing times of around 60 min during any time of the day based on radon measurements within a 40 m high rain forest canopy for the layer between h_c and $0.13 \times h_c$ (canopy top to trunk space). As in the grassland canopy in Mainz Finthen, nighttime in-canopy convection accounted for the small daytime/nighttime variation in their study. Normalization of their canopy flushing time by the layer thickness yielded R_{ac} of the order of $100\,\mathrm{s\,m^{-1}}$, which is around 3–4 times lower than the corresponding R_{ac} of the grassland site. Other studies (Holzinger et al., 2005; Rummel, 2005) based on surface renewal models reported somewhat lower flushing times. Rummel (2005) found flushing times in a 32 m high rain forest canopy of $\leq 200\,\mathrm{s}$ during daytime, which correspond to R_{ac} values $\leq 10\,\mathrm{s\,m^{-1}}$. In the same way Holzinger et al. (2005) determined flushing times of 90 s during daytime and around 300 s during nighttime within a 6 m high scrubby pine forest. Corresponding R_{ac} values were of the order of 20 and $60\,\mathrm{s\,m^{-1}}$, respectively.

Thus, it is important to note that even if the canopy height of natural grassland canopies is small compared to forests (around 1–10 %); the corresponding canopy flushing times are within the same order of magnitude as those reported for forest canopies. The typically high biomass density in the lower canopy of grasslands (e.g. Jäggi et al., 2006; Nemitz et al., 2009) is the most obvious explanation. It provides a large aerodynamic resistance ($> 900\,\mathrm{s\,m^{-1}}$) in a small layer adjacent to the ground (here: $R_{ac}(L_1)$). This resistance is large enough to increase the overall aerodynamic resistance of the whole canopy (R_{ac}) by 50 and 140 % during night and daytime, respectively. Consequently, R_{ac} of the grassland canopy was found to be at least 3–4 times higher than R_{ac} values representing corresponding in-canopy layers of forests taken from the literature.

Plake and Trebs (2013) compared their directly measured transport times with the parameterizations of van Pul and Jacobs (1994) and Personne et al. (2009). They found that none of the parameterizations was able to reproduce the entire diurnal course of the in-canopy transport. Agreement with the measured transport times was either found during daytime (Personne et al., 2009) or nighttime (van Pul and Jacobs, 1994), underlining the need for more direct measurements of in-canopy transport.

4.2 Chemical timescales

The non-linear profiles of NO, NO_2 and O_3 might have introduced uncertainties in $\tau_{ch}(L_{1-3})$. The potential uncertainties due to averaging were investigated by determining the
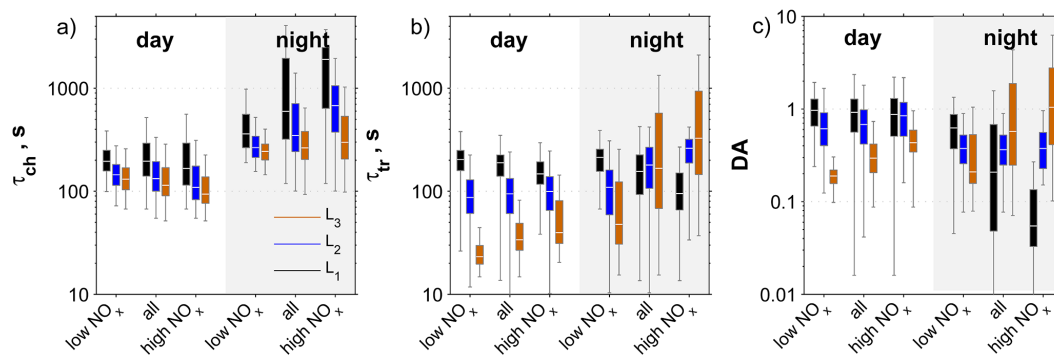
Figure 6. Comparison of box plot statistics for $\tau_{ch}(L_{1-3})$, $\tau_{tr}(L_{1-3})$ and $DA(L_{1-3})$ during daytime and nighttime including all data from 19 August until 26 September 2011 separated for the low and high NO_x periods at the Mainz Finthen grassland site.
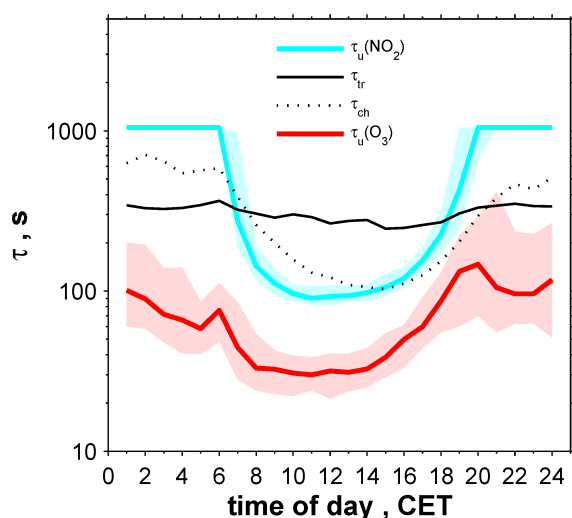
Figure 7. Comparison of median diurnal $\tau_u(NO_2)$, $\tau_u(O_3)$, τ_{tr} and τ_{ch} with interquartile ranges for the whole canopy layer (L_{1+2}) considering all data from 19 August to 26 September 2011 at the Mainz Finthen grassland site.

individual $\tau_{ch}(z_{1-4})$ and their subsequent comparison with $\tau_{ch}(L_{1-3})$. In L_1, L_2 and L_3 they were found to be ≤ 13, ≤ 4 and $\leq 2\%$, respectively, during daytime under any condition. During nighttime, the uncertainties in L_2 and L_3 were found to be 6 and 2% during the low NO_x periods and 57 and 13% during the high NO_x periods, respectively. In L_1 the uncertainty during nighttime was 30% for all conditions. Furthermore, the in-canopy parameterization of j_{NO_2} might have introduced additional uncertainties since (i) in reality the attenuation of in-canopy radiation might be more complex than described in Eq. (3), and (ii) the parameterization of j_{NO_2} from G is prone to uncertainties of $> 40\%$ for $G < 100\,W\,m^{-2}$, 10 – 40 % for $G = 100$–$500\,W\,m^{-2}$ and $\leq 10\%$ for $G > 500\,W\,m^{-2}$ (Trebs et al., 2009). Moreover, omitting the influence of peroxy radical ($HO_2 + RO_2$) levels for the calculation of the chemical timescales introduces

uncertainties. However, measurements of vertical profiles of $HO_2 + RO_2$ inside and above the grassland canopy are challenging and were not made during our experiment. Additionally, no straightforward analytical framework exists to calculate their influence on chemical timescales due to the variety of compounds and reaction rates involved in the complex HO_2 / RO_2 chemistry, which would require numeral modelling (see Heal et al., 2001).

The diurnal maxima and minima of $\tau_{ch}(L_{1-3})$ (Fig. 3a, d, g) were found to coincide with the O_3 minima and maxima (Fig. 2e, f), respectively. The impact of the terms in Eq. (2) on $\tau_{ch}(L_3)$ was examined by a correlation coefficient analysis. It was found to be highest for O_3 followed by NO_2 and NO with $r = -0.57$, $r = 0.46$ and $r = -0.07$, respectively. Consequently, the chemical timescale is dominated by the influence of O_3 as long as O_3 is present in excess compared to the other compounds. As the average air-chemical conditions in Mainz Finthen were characterized by a surplus of O_3 compared to NO_2 or NO (see Sect. 3.2), the magnitude of $\tau_{ch}(L_3)$ was most affected by the mixing ratios of O_3. In contrast, NO was generally less abundant, which explained the low overall impact on $\tau_{ch}(L_3)$. Only during high NO_x periods, when NO levels were above 5 ppb (see Sect. 3.1), was an increased impact of NO on $\tau_{ch}(L_3)$ found.

Figure 6a summarizes the chemical timescales. The temporal variation in τ_{ch}, expressed by higher nighttime and lower daytime values, can be considered as a rather typical pattern based on the diurnal courses of NO, NO_2 and O_3 (Fig. 2e–j) and their strong photochemical link. The vertical variation in $\tau_{ch}(L_{1-3})$ was on the one hand caused by the attenuation of j_{NO_2} in the canopy, and on the other hand by generally increasing mixing ratios of NO, NO_2 and O_3 with height (Fig. 2e–j). It should be noted that the latter finding is exclusively valid for this experimental site. Plake et al. (2014) measured insignificant soil biogenic NO emissions, underlined by weak in-canopy NO gradients (Fig. 2g, h). As already discussed in the previous paragraph, generally low NO, NO_2 and O_3 mixing ratios tend to cause high τ_{ch} values and vice versa. Consequently, at a site with higher NO

emissions, such as an intensively managed agricultural field, the vertical τ_{ch} profile would most likely feature smaller vertical differences.

The extremely high $\tau_{ch}(L_1,)$ during nighttime of the high NO$_x$ periods (Fig. 6a) were a direct consequence of canopy decoupling (see Sect. 4.1.1). Transport of O$_3$ and NO$_2$ into the lower canopy was suppressed by the temperature inversion (see Fig. 2f, j). The residual O$_3$ and NO$_2$ molecules were convectively circulated within the lower canopy and subsequently deposited efficiently to surfaces until both almost disappeared in the early morning (Fig. 2f, j). Consequently, both the negligible NO emissions and the suppressed supply of O$_3$ and NO$_2$ from above yielded very low mixing ratios of all three trace gases, that in turn led to the very high $\tau_{ch}(L_1,)$ values.

Our results are in line with those of Stella et al. (2013) who reported median diurnal τ_{ch} of 80–300 and 150–600 s above and within the canopy, respectively, for an intensively managed meadow. Their in-canopy τ_{ch} maximum was somewhat lower than in Mainz Finthen, which might be attributed to NO soil emissions or to averaging of different layers.

As mentioned above, the chemistry of HO$_2$ / RO$_2$ is not considered in our study. The reaction rate constant of NO + HO$_2$ / RO$_2$ is about 500 times higher than that of the reaction NO + O$_3$. Assuming relatively high average daytime HO$_2$ + RO$_2$ mixing ratios of 60 ppt inside the canopy (see Wolfe et al., 2014) the oxidation of NO to NO$_2$ would be as fast as with 30 ppb of O$_3$. This implies that these chemical timescales may be comparable to those of the reaction NO + O$_3$, which dominates τ_{ch} derived from Eq. (2). However, it should be noted that peroxides have a high affinity to be lost at surfaces, which may reduce their presence in dense grassland canopies. Additionally, reactions between volatile organic compounds (VOCs) and O$_3$ (e.g. Atkinson and Arey, 2003) might have influenced chemical timescales. Simultaneously measured biogenic VOC mixing ratios featured very small values at our site (e.g. isoprene < 0.7 ppb, monoterpene < 0.3 ppb, J. Kesselmeier, personal communication, 2013). Due to the absence of measurements the influence of anthropogenic VOCs is not taken into account.

## 4.3	Influence of meteorology and air pollution on vertical Damköhler number profiles

The summarized daytime $DA(L_{1-3})$ in Fig. 6c exhibited decreasing DA values with increasing layer height. Thus, the likelihood of chemical flux divergence decreased from L_1 to L_3. Throughout L_1 to L_3, the τ_{ch} values (Fig. 6a) showed a lower variation compared to the corresponding τ_{tr} values (Fig. 6b). Hence, the daytime DA profile was mainly caused by the vertical τ_{tr} profile.

Interestingly, the nighttime DA for all data and the high NO$_x$ periods showed opposite vertical profiles, indicating an increasing likelihood of chemical flux divergence with increasing layer height (L_1 to L_3). This was especially pro-

nounced during nighttime of the high NO$_x$ periods, where the only instance without indication for a flux divergence within the entire data set for L_1 was found. The reasons for this were (i) the very high $\tau_{ch}(L_1)$ (Fig. 6a and Sect. 4.2), and (ii) the reversed vertical transport time profiles during nighttime (fastest in L_1) of the high NO$_x$ periods (Fig. 6b). This finding agrees very well with Rummel (2005) who found that the transport timescale in the lowermost layer of an Amazonian rainforest is faster than the chemical timescale of the NO–NO$_2$–O$_3$ triad during nighttime.

Above the canopy, the order of magnitude (Fig. 6c) and the median diurnal course (Fig. 3c) of DA compared well with the values of Stella et al. (2013). The in-canopy DA of Stella et al. (2013) was smaller than the DA above the canopy throughout the entire day, which is in contrast to our study. Considering the average canopy flushing time given in Plake and Trebs (2013) (see Sect. 4.1.2) and the $\tau_{ch}(L_2)$ (see Fig. 6a), the average in-canopy DA in Mainz Finthen was in the order of 2 and 1 for daytime and nighttime, respectively. Thus, in our study in-canopy DA values are on average significantly higher than above the canopy throughout the day. Finally, it should be noted that in-canopy DA values may not be fully representative as besides transport and chemistry, additional sources and sinks for trace gases exist within plant canopies. These are specific for each trace gas and will be further discussed below.

## 4.4	Implications for measured fluxes

### 4.4.1	Potential NO$_x$ canopy reduction

Within the canopy, $DA(L_{1-2})$ (Fig. 3f, i; Fig. 6c) suggest that chemical reactions exhibited a larger influence on the NO–NO$_2$–O$_3$ triad during daytime than during night. However, reactive traces gases in canopies are deposited to soil and vegetation elements. Trace gases can be efficiently taken up by plants due to adsorption/absorption on cuticles and diffusion through stomata (e.g. Breuninger et al., 2012). On the other hand, particularly NO is simultaneously produced by microbial processes and is subsequently released from soil. Although the latter process could be neglected in this study due to insignificant NO soil emissions (Sect. 4.2), the uptake of NO$_2$ by plants, however, was investigated in order to draw conclusions on potential NO$_x$ canopy reduction within natural grasslands canopies. Hence, the characteristic timescale of plant uptake (τ_u) of NO$_2$ integrated over the whole canopy (L_{1+2}) was estimated based on a resistance model (Baldocchi, 1988), following an approach of Rummel (2005) as

$$\tau_u(x) = \left(\frac{1}{R_{L_x}} \times \frac{\Delta LAI}{\Delta z} \right)^{-1}, \qquad (7)$$

where x denotes the trace gas of interest (here $x = $ NO$_2$) and R_{L_x} is the leaf resistance of x:

$$R_{L_x} = \left(\frac{1}{R_{bl_x} + R_{s_x} + R_{mes_x}} + \frac{2}{R_{bl_x} + R_{cut_x}} \right)^{-1}, \qquad (8)$$

with R_{bl_x} being the leaf boundary layer resistance of x calculated according to Personne et al. (2009), R_{s_x} the stomatal resistance of x taken from Plake et al. (2014), R_{mes_x} the mesophyll resistance set to $200\,\mathrm{s\,m^{-1}}$ for NO_2 and R_{cut_x} the cuticular resistance set to $9999\,\mathrm{s\,m^{-1}}$ due to the unimportance of cuticular deposition for NO_2 (both values were taken from Stella et al., 2013).

During daytime, the median of $\tau_u(NO_2)$ calculated from all data was typically found to be the shortest amongst all timescales relevant for NO_2, typically ranging between 90 and $160\,\mathrm{s}$ between 09:00 and 17:00 CET (Fig. 7). This timescale was closely followed by $\tau_{ch}(L_{1+2})$ exhibiting values between 100 and $200\,\mathrm{s}$ in the same time period, but the minimum was slightly skewed towards the afternoon. In contrast, the canopy flushing time, $\tau_{tr}(L_{1+2})$, ranged from 250 to $290\,\mathrm{s}$ (Fig. 7) during this time. For a comparable natural grassland canopy with significant NO soil emissions, this would imply an efficient in-canopy conversion of NO to NO_2 during daytime, followed by an effective NO_2 plant uptake as the transport was found to be 2–3 times slower. Furthermore, the biomass density within the lowest $0.2\,\mathrm{m}$ of the canopy (i) strongly inhibits the transport, especially in L_1 during daytime (Figs. 5; 6b), and (ii) attenuates the photolysis of NO_2 at the soil–canopy interface, the location where NO is usually emitted. This indicates that a strong potential for NO_x canopy reduction exists in such grassland ecosystems during daytime, when the precondition of significant NO soil emissions is fulfilled. The presence of peroxy radicals may even amplify this process.

However, during nighttime, $\tau_u(NO_2)$ was found to be very large (Fig. 7) due to plant stomata closure. Hence, the role of turbulence–chemistry interactions ($DA(L_{1-2})$) was dominating over biological uptake processes. In L_1 the transport of soil emitted NO would be slowest under relatively windy nighttime situations (low NO_x periods in Fig. 3h) due to undeveloped in-canopy convection. Thus, a considerably high mixing ratio of O_3 within the canopy (Fig. 2e) would lead to an efficient formation of NO_2 indicated by $DA(L_{1-2})$ close to unity. The uptake of NO_2 by plants would be insignificant (see above), and only soil deposition would lead to a small NO_2 depletion. Most likely, such nighttime conditions would lead to simultaneous NO_2 and NO canopy emission fluxes. During nights with low wind speeds (high NO_x periods), the temperature inversion constitutes a "canopy lid". Within the canopy (L_{1+2}) the reaction of residual O_3 (see Sect. 4.2) and soil-emitted NO would compete with the O_3 deposition to surfaces. Subsequently, a mixture of NO and NO_2 would be trapped inside the canopy. Besides some minor in-canopy NO_2 losses (see above), a distinct NO and NO_2 release may occur in the morning hours, which has been observed for forests (see Foken et al., 2012; Dorsey et al., 2004; Jacob and Wofsy, 1990).

4.4.2 Influence on O_3 deposition flux

Similar to NO_2, the application of in-canopy DA values for O_3 remains difficult, since plant uptake and deposition to plant surfaces and the soil are additional O_3 loss pathways. The characteristic timescale of O_3 plant uptake and soil deposition $\tau_u(O_3)$, shown in Fig. 7, was estimated using Eqs. (7) and (8), with $x = O_3$, R_{mes_x} set to $0\,\mathrm{s\,m^{-1}}$ (Erisman et al., 1994) and $R_{cut_x} = R_{ns_x} - R_{soil_x}$ (e.g. Lamaud et al., 2009). The R_{ns_x} was taken from Plake et al. (2014) and $R_{soil_x} = 240\,\mathrm{s\,m^{-1}}$ according to Lamaud et al. (2009). The $\tau_u(O_3)$ ranged from 30 to $150\,\mathrm{s}$, which clearly illustrates the dominance of in-canopy O_3 plant uptake and soil deposition. The $\tau_u(O_3)$ was significantly faster than both $\tau_{tr}(L_{1-2})$ and $\tau_{ch}(L_{1-2})$ during the entire day (values are given in Sect. 4.4.1).

Consequently, only DA values above the canopy, i.e. $DA(L_3)$, provide an indication for potential O_3 flux divergence. Since the $DA(L_3)$ always exceeded 0.1 (Figs. 3c, 6c), a chemical flux divergence could not be excluded at the Mainz Finthen site. Furthermore, $DA > 1$ (Fig. 3c) during the early evening hours clearly indicated the dominance of chemical reactions over transport. During the low NO_x periods, the probability for flux divergence was lowest. The influence of chemistry on O_3 deposition fluxes determined by Plake et al. (2014) at the Mainz Finthen grassland site will be discussed below. The median O_3 fluxes for the entire measurement period ranged from about -1.5 to $-6\,\mathrm{nmol\,m^2\,s^{-1}}$ during night and daytime, respectively.

Due to negligible NO soil emissions, a chemical flux divergence in L_3 resulting from counter-directed fluxes of NO and O_3 was very unlikely. Nevertheless, we use a simplified method proposed by Duyzer et al. (1995) based on R1 and R3 and the law of mass conservation to approximate the flux divergence by the correction factor α_{O_3} as

$$\alpha_{O_3} = \frac{\phi_x}{\kappa \times u_*} \times [k_1 \times (N_{NO} \times F_{O_3}^* + N_{O_3} \times F_{NO}^*) - j_{NO_2} \times F_{NO_2}^*], \quad (9)$$

where $\phi_x = \phi_{O_3} = \phi_H$ was the stability correction function for heat (Högström, 1988), $F_{O_3}^*$ the measured O_3 flux at z_{ref} determined by the eddy covariance method (see Plake et al., 2014) and F_{NO}^* and $F_{NO_2}^*$ the corresponding NO and NO_2 fluxes determined by the dynamic chamber technique (see Plake et al., 2014). The estimated O_3 deposition flux at z_3 (F_{z_3}) was then calculated as

$$F_{z_3} = F_{z_{ref}} + \int_{z_3}^{z_{ref}} \left(\frac{\partial F}{\partial z}\right)_z \mathrm{d}z = F_{O_3}^* + \alpha_{O_3} \times z_3 \times \left(1 + \ln \frac{z_{ref}}{z_3}\right), \quad (10)$$

where the term $\int_{z_3}^{z_{ref}} \left(\frac{\partial F}{\partial z}\right)_z \mathrm{d}z$ is the integrated flux divergence within L_3. The resulting median O_3 flux divergence was quantified to be less than 1 %, confirming our a priori assumption.
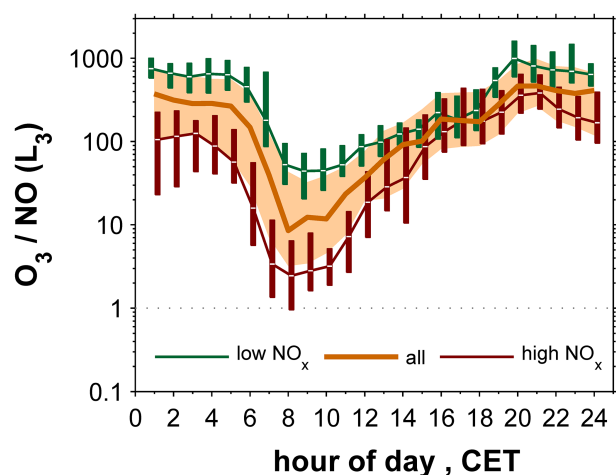
Figure 8. Diurnal course of the O_3 to NO ratio in L_3 considering all data from 19 August to 26 September 2011 (median and shaded interquartile range) and separated for the low NO_x and high NO_x periods (medians and interquartile boxes) at the Mainz Finthen grassland site.

Nevertheless, we examined the influence of the enhanced NO mixing ratios in the morning hours (Sect. 3.2, Fig. 2g, h), accompanied by very low O_3 / NO ratios (Fig. 8) on the measured O_3 fluxes. A chemically induced O_3 flux $F_c(O_3)$ due to production $P(O_3)$ or loss $L(O_3)$ of O_3 by Reactions (R1) and (R3) integrated over the air column of L_3 was quantified according to Rummel et al. (2007) as

$$F_c(O_3) = P(O_3) - L(O_3) = \int_{z_3}^{z_{ref}} \frac{\mu_{NO_2}(z) \times \rho_d(z)}{\tau_{NO_2}(z)} dz$$

$$- \int_{z_3}^{z_{ref}} \frac{\mu_{O_3}(z) \times \rho_d(z)}{\tau_{O_3}(z)} dz, \tag{11}$$

where ρ_d (in mol m^{-3}) is the molar density of dry air. τ_{NO_2} and τ_{O_3} (in s) are the chemical depletion times of NO_2 and O_3, respectively:

$$\tau_{NO_2} = \frac{1}{j_{NO_2}} \tag{12}$$

$$\tau_{O_3} = \frac{1}{k_1 \times N_{NO}}. \tag{13}$$

Figure 9a displays the diurnal courses of $P(O_3)$ and $L(O_3)$ exhibiting median values of 0 to 1.9 nmol m^{-2} s^{-1} and 0 to -1.4 nmol m^{-2} s^{-1}, respectively. The maximal median values were related to the enhanced NO_x levels in the morning. The resulting median net $F_c(O_3)$ in Fig. 9b ranged between 0.6 and -0.05 nmol m^{-2} s^{-1}, representing a net O_3 production in L_3 during daytime and a net loss during nighttime. Repeatedly, the medians of low and high NO_x periods

adjoined the interquartile range of the overall data set, showing a variability of one order of magnitude of net $F_c(O_3)$ during daytime. Considering the median values of all data, the chemical contribution to the measured EC flux of O_3 would be around $+10\%$ during daytime and -3% during nighttime. Consequently, the actual daytime O_3 deposition to the canopy is higher than measured by the EC method. This finding is interesting, as to our knowledge previous studies only reported chemical O_3 losses above the canopy due to outbalancing of the reactions of O_3 with NO (e.g. Dorsey et al., 2004) or VOCs (e.g. Kurpius and Goldstein, 2003) emitted by soil or plants, respectively. The net O_3 production in our study was attributed to a deviation from the NO–NO_2–O_3 photostationary state by a surplus of NO_2 due to NO oxidation by e.g., peroxy radicals or other oxidants (see Trebs et al., 2012). Unfortunately, we were not able to assess the impact of the reactions involved in the net O_3 production on the calculated chemical timescales as measurements of peroxy radicals were not available. The NO_2 surplus might have originated from simultaneous emissions of non-methane hydrocarbons, carbon monoxide (CO) and NO from motorways surrounding the site in a distance of some kilometres. It is well known that under daytime conditions peroxy radicals are formed that can oxidize NO without consumption of O_3 resulting in net O_3 production (Seinfeld and Pandis, 2006). Although this O_3 production might also prevail at other experimental sites, this effect is most likely balanced or even exceeded by the destruction of O_3 due to biogenic soil NO emissions which were negligible at our site (a nutrient-poor grassland site).

5 Conclusions

For the first time, we simultaneously measured transport times (aerodynamic resistances), vertical profiles of NO–NO_2–O_3 mixing ratios and micrometeorological quantities within and above a natural grassland canopy. The obtained data were analysed to gain insights about the potential NO_x canopy reduction in the grassland canopy, and to analyse the contribution of chemistry on fluxes of purely depositing compounds, such as O_3. We observed two extreme regimes: (a) high wind speed and low NO_x mixing ratios (low NO_x periods) and (b) low wind speed and high NO_x mixing ratios (high NO_x periods). Our study highlights that as a result of in-canopy convection, nighttime transport in the lowermost canopy layer is fastest, while conditions above the canopy are highly stable due to low wind speed during the high NO_x periods.

Interestingly, our results on transport-chemistry interactions within the grassland canopy are partly comparable to those found in the Amazonian rainforest, although the vertical canopy structure differs substantially. Natural grasslands exhibit very high biomass densities in the lowest part of the canopy. Thus, the median aerodynamic resistance in the low-
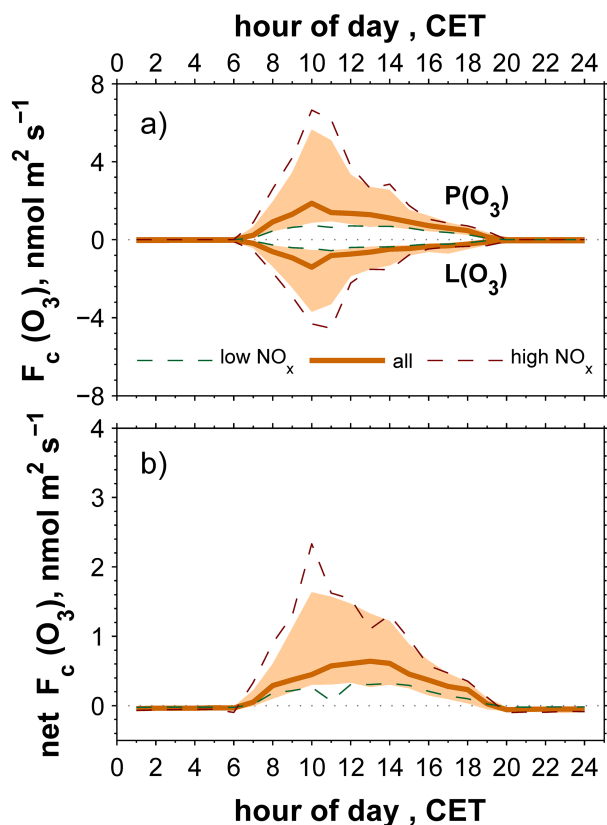
Figure 9. Diurnal courses showing **(a)** $P(O_3)$ and $L(O_3)$ and **(b)** $F_c(O_3)$ (Eq. 11) for L_3 considering all days from 19 August to 26 September 2011 (medians and shaded interquartile ranges) and separated for the low and high NO_x periods (medians) at the Mainz Finthen grassland site.

ermost canopy layer (0.04–0.2 m) was found to be of the same magnitude ($> 900\,\mathrm{s\,m^{-1}}$) and to feature the same diurnal pattern (higher during daytime, lower at night) as the aerodynamic resistance determined for the lowest metre of an Amazonian rain forest. The median in-canopy aerodynamic resistance representing the whole grassland canopy was at least 3–4 times higher than in-canopy aerodynamic resistances of forest canopies available from the literature. Our results reveal that even if the canopy height of natural grassland canopies is small compared to forests (around 1–10 %), the corresponding canopy flushing times are of the same order of magnitude as those reported for forest canopies. The median canopy flushing times exhibited only small daytime/nighttime variability, which is in accordance with a detailed study on flushing times within an Amazonian rain forest (Simon et al., 2005). The small daytime/nighttime variability is caused by the compensating transport efficiencies in the lower and upper canopy layers during daytime and nighttime for both canopy types.

The median canopy flushing time of the grassland was found to be $\leq 6\,\mathrm{min}$ and the chemical timescale of the NO–

NO_2–O_3 triad during daytime ranged between 1–3 min. This has obvious implications, e.g. for soil-emitted reactive compounds such as NO, potentially implying fast chemical conversion of NO to NO_2 within the grassland canopy. During daytime the plant uptake of NO_2 was shown to be 2–3 times faster than the canopy flushing time. Inevitably, this leads to a strong potential NO_x canopy reduction in the presence of biogenic NO soil emissions. This effect may be amplified if substantial levels of peroxy radicals prevail inside the canopy. Due to the extensive global terrestrial coverage with grassland canopies, this finding is highly relevant for the application of global chemistry and transport models. Our results indicate that the daytime NO_x canopy reduction for grasslands may be higher than 64 %. Nevertheless, an improved daily average for the NO_x canopy reduction factor in analogy to Yienger and Levy (1995) cannot be presented here due to the insignificant NO soil emissions at the experimental site.

Moreover, we determined a median net chemical O_3 production of 10 % during daytime within the air column between the EC flux measurement and the canopy, which was due to the absence of soil biogenic NO emission in our study. Hence, in contrast to previous studies our measured O_3 deposition flux by EC is slightly underestimated. The chemical flux divergence for O_3 was one order of magnitude larger during the high NO_x than during the low NO_x periods. In-canopy Damköhler numbers were shown to be relevant for NO_2 only under nighttime conditions, which was due to the minor role of NO_2 uptake by plants at this time. Damköhler numbers above the canopy indicated a potential flux divergence, but did not provide a hint for the observed chemical production of O_3. The only instance without indication of a chemical flux divergence within the entire data set was found during nighttime of the high NO_x periods in the lowermost canopy layer.

References

Atkinson, R. and Arey, J.: Gas-phase tropospheric chemistry of biogenic volatile organic compounds: a review, Atmos. Environ., 37, S197–S219, 2003.

Atkinson, R., Baulch, D. L., Cox, R. A., Crowley, J. N., Hampson, R. F., Hynes, R. G., Jenkin, M. E., Rossi, M. J., and Troe, J.:

Evaluated kinetic and photochemical data for atmospheric chemistry: Volume I – gas phase reactions of O_x, HO_x, NO_x and SO_x species, Atmos. Chem. Phys., 4, 1461–1738, doi:10.5194/acp-4-1461-2004, 2004.

Aylor, D. E., Wang, Y. S., and Miller, D. R.: Intermittent wind close to the ground within a grass canopy, Bound.-Lay. Meteorol., 66, 427–448, 1993.

Bakwin, P. S., Wofsy, S. C., Fan, S. M., Keller, M., Trumbore, S. E., and Dacosta, J. M.: Emission of nitric-oxide (NO) from tropical forest soils and exchange of NO between the forest canopy and atmospheric boundary-layers, J. Geophys. Res.-Atmos., 95, 16755–16764, 1990.

Baldocchi, D.: A multi-layer model for estimating sulfur-dioxide deposition to a deciduous oak forest canopy, Atmos. Environ., 22, 869–884, 1988.

Breuninger, C., Oswald, R., Kesselmeier, J., and Meixner, F. X.: The dynamic chamber method: trace gas exchange fluxes (NO, NO_2, O_3) between plants and the atmosphere in the laboratory and in the field, Atmos. Meas. Tech., 5, 955–989, doi:10.5194/amt-5-955-2012, 2012.

Crutzen, P.: Discussion of chemistry of some minor constituents in stratosphere and troposphere, Pure Appl. Geophys., 106, 1385–1399, 1973.

Denmead, O. T., Freney, J. R., and Dunin, F. X.: Gas exchange between plant canopies and the atmosphere: Case-studies for ammonia, Atmos. Environ., 42, 3394–3406, 2007.

Dorsey, J. R., Duyzer, J. H., Gallagher, M. W., Coe, H., Pilegaard, K., Weststrate, J. H., Jensen, N. O., and Walton, S.: Oxidized nitrogen and ozone interaction with forests, I: Experimental observations and analysis of exchange with Douglas fir, Q. J. Roy Meteor. Soc., 130, 1941–1955, 2004.

Dupont, S. and Patton, E. G.: Momentum and scalar transport within a vegetation canopy following atmospheric stability and seasonal canopy changes: the CHATS experiment, Atmos. Chem. Phys., 12, 5913–5935, doi:10.5194/acp-12-5913-2012, 2012.

Duyzer, J. H., Deinum, G., and Baak, J.: The interpretation of measurements of surface exchange of nitrogen-oxides – correction for chemical-reactions, Philos. T. R. Soc. A, 351, 231–248, 1995.

Erisman, J. W., Vanpul, A., and Wyers, P.: Parametrization of surface-resistance for the quantification of atmospheric deposition of acidifying pollutants and ozone, Atmos. Environ., 28, 2595–2607, 1994.

Finnigan, J.: Turbulence in plant canopies, Annu. Rev. Fluid Mech., 32, 519–571, 2000.

Foken, T.: Micrometeorology, Springer, Berlin, Heidelberg, 306 pp., 2008.

Foken, T., Meixner, F. X., Falge, E., Zetzsch, C., Serafimovich, A., Bargsten, A., Behrendt, T., Biermann, T., Breuninger, C., Dix, S., Gerken, T., Hunner, M., Lehmann-Pape, L., Hens, K., Jocher, G., Kesselmeier, J., Luers, J., Mayer, J. C., Moravek, A., Plake, D., Riederer, M., Rutz, F., Scheibe, M., Siebicke, L., Sörgel, M., Staudt, K., Trebs, I., Tsokankunku, A., Welling, M., Wolff, V., and Zhu, Z.: Coupling processes and exchange of energy and reactive and non-reactive trace gases at a forest site – results of the EGER experiment, Atmos. Chem. Phys., 12, 1923–1950, doi:10.5194/acp-12-1923-2012, 2012.

Ganzeveld, L., Ammann, C., and Loubet, B.: Review on modelling atmosphere biosphere ex-change of Ozone and Nitrogen oxides. Background document for the joint ÉCLAIRE/COST ES0804

Expert Workshop "From process scale to global scale: integrating our knowledge on biosphere/atmosphere exchange modelling of trace gases and volatile aerosols", 2012.

Gut, A., Scheibe, M., Rottenberger, S., Rummel, U., Welling, M., Ammann, C., Kirkman, G. A., Kuhn, U., Meixner, F. X., Kesselmeier, J., Lehmann, B. E., Schmidt, W., Muller, E., and Piedade, M. T. F.: Exchange fluxes of NO_2 and O_3 at soil and leaf surfaces in an Amazonian rain forest, J. Geophys. Res.-Atmos., 107, 8060, doi:10.1029/2001JD000654, 2002.

Hänsel, H. and Neumann, W.: Physik, Spectrum, Akad. Verl., Heidelberg, Berlin, Oxford, 1995.

Heal, M. R., Booth, B. B. B., Cape, J. N., and Hargreaves, K. J.: The influence of simplified peroxy radical chemistry on the interpretation of NO_2-NO-O_3 surface exchange, Atmos. Environ. 35, 1687–1696, 2001.

Hicks, B. B., Baldocchi, D. D., Meyers, T. P., Hosker, R. P., and Matt, D. R.: A preliminary multiple resistance routine for deriving dry deposition velocities from measured quantities, Water Air Soil Poll., 36, 311–330, 1987.

Högström, U.: Non-dimensional wind and temperature profiles in the atmospheric surface-layer – a re-evaluation, Bound.-Lay. Meteorol., 42, 55–78, 1988.

Holzinger, R., Lee, A., Paw, K. T., and Goldstein, U. A. H.: Observations of oxidation products above a forest imply biogenic emissions of very reactive compounds, Atmos. Chem. Phys., 5, 67–75, doi:10.5194/acp-5-67-2005, 2005.

IPCC: Climate Change 2013: the physical science basis. Working group I contribution to the fifth assessment report of the Intergovernmental Panel on Climate Change, University Press, Cambridge, UK, 2013.

Jacob, D. J. and Wofsy, S. C.: Budgets of reactive nitrogen, hydrocarbons, and ozone over the amazon-forest during the wet season, J. Geophys. Res.-Atmos., 95, 16737–16754, 1990.

Jacobs, A. F. G., Vanboxel, J. H., and Elkilani, R. M. M.: Nighttime free-convection characteristics within a plant canopy, Bound.-Lay. Meteorol., 71, 375–391, 1994.

Jäggi, M., Ammann, C., Neftel, A., and Fuhrer, J.: Environmental control of profiles of ozone concentration in a grassland canopy, Atmos. Environ., 40, 5496–5507, 2006.

Kasanko, M., Palmieri, A., and Coyette, C.: Land cover/ land use statistics, in: Agriculture and Fishery Statistics, edited by: Coyette, C., and Schenk, H., Eurostat, Luxembourg, 158, 2011.

Kruijt, B., Malhi, Y., Lloyd, J., Norbre, A. D., Miranda, A. C., Pereira, M. G. P., Culf, A., and Grace, J.: Turbulence statistics above and within two Amazon rain forest canopies, Bound.-Lay. Meteorol., 94, 297–331, 2000.

Kurpius, M. R. and Goldstein, A. H.: Gas-phase chemistry dominates O_3 loss to a forest, implying a source of aerosols and hydroxyl radicals to the atmosphere, Geophys. Res. Lett., 30, 1371, doi:10.1029/2002gl016785, 2003.

Lamaud, E., Loubet, B., Irvine, M., Stella, P., Personne, E., and Cellier, P.: Partitioning of ozone deposition over a developed maize crop between stomatal and non-stomatal uptakes, using eddy-covariance flux measurements and modelling, Agr. Forest Meteorol., 149, 1385–1396, 2009.

Lehmann, B. E., Lehmann, M., Neftel, A., Gut, A., and Tarakanov, S. V.: Radon-220 calibration of near-surface turbulent gas transport, Geophys. Res. Lett., 26, 607–610, 1999.

Lenschow, D. H.: Reactive trace species in the boundary-layer from a micrometeorological perspective, J. Meteorol. Soc. Jpn., 60, 472–480, 1982.

Lerdau, M. T., Munger, L. J., and Jacob, D. J.: Atmospheric chemistry - the NO_2 flux conundrum, Science, 289, 2291, doi:0.1126/science.289.5488.2291, 2000.

Mauder, M. and Foken, T.: Documentation and instruction manual of the eddy-covariance software package TK3, Arbeitsergebnisse Nr. 46, 2011.

Monsi, M. and Saeki, T.: Über den Lichtfaktor in den Pflanzengesellschaften und seine Bedeutung für die Stoffproduktion, Jpn. J. Botany, 14, 22–52, 1953.

Monteith, J. L. and Unsworth, M. H.: Principles of environmental physics, 2nd ed., E. Arnold, London, New York, 291 pp., 1990.

Moravek, A., Foken, T., and Trebs, I.: Application of a GC-ECD for measurements of biosphere–atmosphere exchange fluxes of peroxyacetyl nitrate using the relaxed eddy accumulation and gradient method, Atmos. Meas. Tech., 7, 2097–2119, doi:10.5194/amt-7-2097-2014, 2014.

Moravek, A., Stella, P., Foken, T., and Trebs, I.: Influence of local air pollution on the deposition of peroxyacetyl nitrate to a nutrient-poor natural grassland ecosystem, Atmos. Chem. Phys., 15, 899–911, doi:10.5194/acp-15-899-2015, 2015.

Nemitz, E., Sutton, M. A., Gut, A., San Jose, R., Husted, S., and Schjoerring, J. K.: Sources and sinks of ammonia within an oilseed rape canopy, Agr. Forest Meteorol., 105, 385–404, 2000.

Nemitz, E., Loubet, B., Lehmann, B. E., Cellier, P., Neftel, A., Jones, S. K., Hensen, A., Ihly, B., Tarakanov, S. V., and Sutton, M. A.: Turbulence characteristics in grassland canopies and implications for tracer transport, Biogeosciences, 6, 1519–1537, doi:10.5194/bg-6-1519-2009, 2009.

Personne, E., Loubet, B., Herrmann, B., Mattsson, M., Schjoerring, J. K., Nemitz, E., Sutton, M. A., and Cellier, P.: SURFATM-NH3: a model combining the surface energy balance and bi-directional exchanges of ammonia applied at the field scale, Biogeosciences, 6, 1371–1388, doi:10.5194/bg-6-1371-2009, 2009.

Plake, D. and Trebs, I.: An automated system for selective and continuous measurements of vertical thoron profiles for the determination of transport times near the ground, Atmos. Meas. Tech., 6, 1017–1030, doi:10.5194/amt-6-1017-2013, 2013.

Plake, D., Stella, P., Moravek, A., Mayer, J. C., Ammann, C., Held, A., and Trebs, I.: Comparison of ozone deposition measured with the dynamic chamber and the eddy covariance method, Agr. Forest Meteorol., submitted, 2014.

Rinne, J., Markkanen, T., Ruuskanen, T. M., Petaja, T., Keronen, P., Tang, M. J., Crowley, J. N., Rannik, U., and Vesala, T.: Effect of chemical degradation on fluxes of reactive compounds – a study with a stochastic Lagrangian transport model, Atmos. Chem. Phys., 12, 4843–4854, doi:10.5194/acp-12-4843-2012, 2012.

Ripley, E. A. and Redman, R. E.: Grassland, in: Vegetation and the atmosphere, edited by: Monteith, J. L., Acad. Press, London, 1976.

Rummel, U.: Turbulent exchange of ozone and nitrogen oxides between an Amazonian rain forest and the atmosphere, PhD thesis, Faculty of Biology, Chemistry and Geosciences, University of Bayreuth, Bayreuth, 246 pp., 2005.

Rummel, U., Ammann, C., Gut, A., Meixner, F. X., and Andreae, M. O.: Eddy covariance measurements of nitric oxide flux within an Amazonian rain forest, J. Geophys. Res.-Atmos., 107, 8050, doi:10.1029/2001jd000520, 2002.

Rummel, U., Ammann, C., Kirkman, G. A., Moura, M. A. L., Foken, T., Andreae, M. O., and Meixner, F. X.: Seasonal variation of ozone deposition to a tropical rain forest in southwest Amazonia, Atmos. Chem. Phys., 7, 5415–5435, 2007, http://www.atmos-chem-phys.net/7/5415/2007/.

Seinfeld, J. H. and Pandis, S. N.: Atmospheric chemistry and physics : from air pollution to climate change, 2. Edn., Wiley, Hoboken, NJ, 1203 pp., 2006.

Simon, E., Lehmann, B. E., Ammann, C., Ganzeveld, L., Rummel, U., Meixner, F. X., Nobre, A. D., Araujo, A., and Kesselmeier, J.: Lagrangian dispersion of Rn-222, H_2O and CO_2 within Amazonian rain forest, Agr. Forest Meteorol., 132, 286–304, 2005.

Stella, P., Kortner, M., Ammann, C., Foken, T., Meixner, F. X., and Trebs, I.: Measurements of nitrogen oxides and ozone fluxes by eddy covariance at a meadow: evidence for an internal leaf resistance to NO_2, Biogeosciences, 10, 5997–6017, doi:10.5194/bg-10-5997-2013, 2013.

Suttie, J. M., Reynolds, S. G., and Batello, C.: Introduction, in: Grasslands of the world, edited by: Suttie, J. M., Reynolds, S. G., and Batello, C., FAO, Rome, 2005.

Swinbank, W. C.: A comparison between predictions of dimensional analysis for constant-flux layer and observations in unstable conditions, Q. J. Roy Meteor. Soc., 94, 460–467, 1968.

Trebs, I., Bohn, B., Ammann, C., Rummel, U., Blumthaler, M., Königstedt, R., Meixner, F. X., Fan, S., and Andreae, M. O.: Relationship between the NO_2 photolysis frequency and the solar global irradiance, Atmos. Meas. Tech., 2, 725–739, doi:10.5194/amt-2-725-2009, 2009.

Trebs, I., Mayol-Bracero, O. L., Pauliquevis, T., Kuhn, U., Sander, R., Ganzeveld, L., Meixner, F.X., Kesselmeier, J., Artaxo, P. and Andreae, M. O.: Impact of the Manaus urban plume on trace gas mixing ratios near the surface in the Amazon Basin: Implications for the NO-NO_2-O_3 photostationary state and peroxy radical levels, J. Geophys. Res., 117, D05307, doi:10.1029/2011JD016386, 2012.

Trumbore, S. E., Keller, M., Wofsy, S. C., and Dacosta, J. M.: Measurements of soil and canopy exchange-rates in the Amazon rainforest using Rn-222, J. Geophys. Res.-Atmos., 95, 16865–16873, 1990.

van Pul, W. A. J., and Jacobs, A. F. G.: The conductance of a maize crop and the underlying soil to ozone under various environmental-conditions, Bound.-Lay. Meteorol., 69, 83–99, 1994.

Warneck, P.: Chemistry of the natural atmosphere, 2nd ed., Academic Press, San Diego, California, 927 pp., 2000.

Wolfe, G. M., Cantrell, C., Kim, S., Mauldin III, R. L., Karl, T., Harley, P., Turnipseed, A., Zheng, W., Flocke, F., Apel, E. C., Hornbrook, R. S., Hall, S. R., Ullmann, K., Henry, S. B., DiGangi, J. P., Boyle, E. S., Kaser, L., Schnitzhofer, R., Hansel, A., Graus, M., Nakashima, Y., Kajii, Y., Guenther, A., and Keutsch, F. N.: Missing per-oxy radical sources within a summertime ponderosa pine forest, Atmos. Chem. Phys., 14, 4715–4732, doi:10.5194/acp-14-4715-2014, 2014.

Yienger, J. J. and Levy, H.: Empirical-model of global soil-biogenic NO_x emissions, J. Geophys. Res.-Atmos., 100, 11447–11464, 1995.